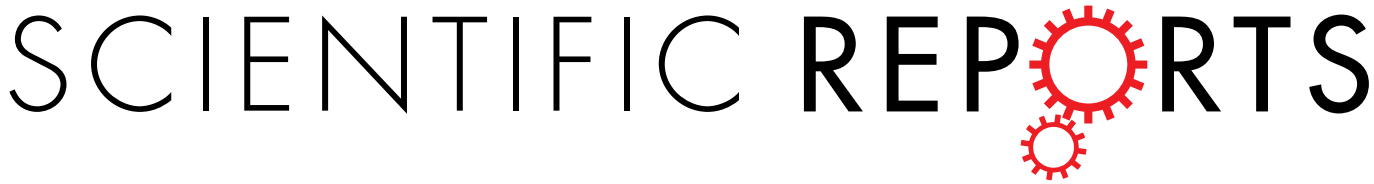

OPEN

Analogy of transistor function with modulating photonic band gap in electromagnetically induced grating

Received: 04 February 2015
Accepted: 06 August 2015
Published: 09 September 2015

Zhiguo Wang[1,2], Zakir Ullah[1], Mengqin Gao[1], Dan Zhang[1], Yiqi Zhang[1], Hong Gao[2] & Yanpeng Zhang[1]

Optical transistor is a device used to amplify and switch optical signals. Many researchers focus on replacing current computer components with optical equivalents, resulting in an optical digital computer system processing binary data. Electronic transistor is the fundamental building block of modern electronic devices. To replace electronic components with optical ones, an equivalent optical transistor is required. Here we compare the behavior of an optical transistor with the reflection from a photonic band gap structure in an electromagnetically induced transparency medium. A control signal is used to modulate the photonic band gap structure. Power variation of the control signal is used to provide an analogy between the reflection behavior caused by modulating the photonic band gap structure and the shifting of Q-point (Operation point) as well as amplification function of optical transistor. By means of the control signal, the switching function of optical transistor has also been realized. Such experimental schemes could have potential applications in making optical diode and optical transistor used in quantum information processing.

In analogy to their electronic counterparts, optical transistors and switches are required as fundamental building blocks for classical as well as quantum optical information processing[1,2]. In particular, an optical transistor and switch operated by a single photon stored in an atomic ensemble inside a cavity has recently been demonstrated[3]. In this article we will theoretically and experimentally demonstrate the analogy of an optical transistor function with the enhancement and suppression of multi-wave mixing process through the modulation of a photonic band gap structure. Four-wave mixing is a well-known nonlinear optical effect which can be enhanced in an electromagnetically-induced transparency (EIT) medium[4–6]. Four wave mixing[7–10] and six wave mixing[11] have been individually studied in multi-level atomic systems. By choosing appropriate atomic level schemes and driving fields, one can generate controllable nonlinearities with very interesting applications in designing novel nonlinear optical devices. This motivates the studies of enhanced higher-order nonlinear wave-mixing processes. Enhanced six-wave mixing via induced atomic coherence was experimentally observed in a four level inverted Y-type atomic system[12]. Such six-wave mixing signal can be made to even coexist, compete, and spatially interfere with the four-wave mixing signal in the same system[13] by the assistance of EIT. The EIT-based nonlinear schemes can be driven both by traveling wave beams and standing wave beams. The large nonlinearity was obtained in an atomic system driven by two counter propagating coupling fields of the same frequency which form a standing wave[14,15]. Standing wave interacts with atomic coherent medium to result in an electromagnetically induced grating[16,17]. The electromagnetically induced grating possesses

[1]Key Laboratory for Physical Electronics and Devices of the Ministry of Education & Shaanxi Key Lab of Information Photonic Technique, Xi'an Jiaotong University, Xi'an 710049, China. [2]School of Science, Xi'an Jiaotong University, Xi'an 710049, China. Correspondence and requests for materials should be addressed to Z.W. (email: wangzg@mail.xjtu.edu.cn) or Y.Z. (email: ypzhang@mail.xjtu.edu.cn)

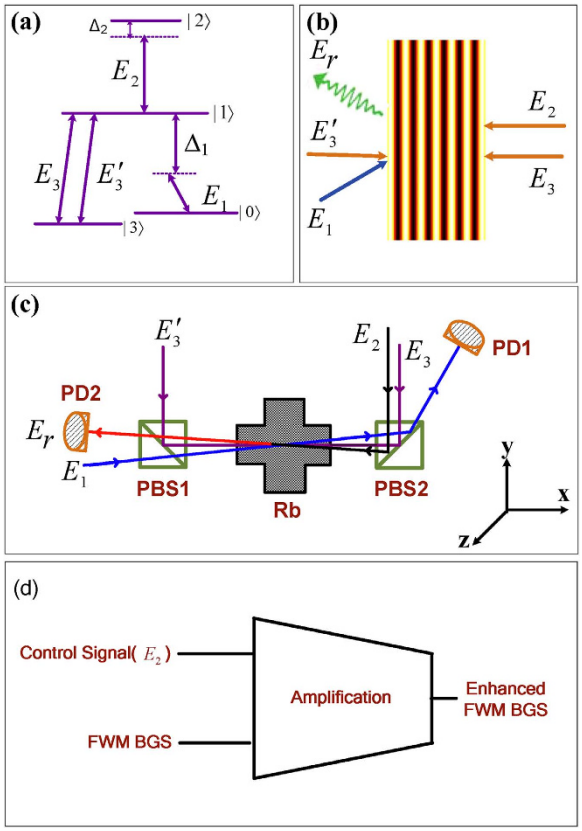

Figure 1. (**a**) Four-level energy system. (**b**) Schematic of an electromagnetically induced grating formed by two coupling beams E_3 and E_3'. Together with the dressing field E_2 and probe field E_1, a dressed band gap signal E_r will be generated according to the phase-matching condition $\mathbf{k_r} = \mathbf{k_1} - \mathbf{k_3'} + \mathbf{k_3}$. (**c**) The setup of our experiment. (**d**) Block diagram of the analogy of transistor amplification function.

a photonic band gap structure as shown in Fig. 1(c). Such electromagnetically induced grating has potential applications in manipulation of light propagation to create tunable photonic band gap structures[18–20]. Moreover the relevant research can also be used to make optical diodes if the photonic crystal induced in the medium from periodic modulation of its optical properties is set into motion[21].

In this letter, we report the optical response of rubidium (^{85}Rb) atomic vapors driven by a standing wave coupling field and probe field, from which the optically controllable photonic band gap structure can be generated. We report an experimental and theoretical demonstration of the reflection from a photonic band gap structure along with probe transmission signal in EIT based inverted Y-type four level atomic system. We show four-wave mixing band gap signal (FWM BGS) can be suppressed and enhanced. The suppressed and enhanced FWM BGS can be used to provide an analogy with the switching and amplification functions of an optical transistor. The probe frequency detuning is used to find the optimal experimental conditions for the reflected band gap signal. The periodic energy levels generated by the standing wave under EIT condition are further modulated with the help of a control signal to exploit the photonic band gap structure and change the reflectivity. Manipulating the photonic band gap structure with the help of a control signal and changing power of the incident probe field are the two alternative ways used to change intensity of the reflection from a photonic band gap structure.

Results

The experiment was carried out in a cell contained rubidium (^{85}Rb) atomic vapors for a simple inverted Y-type atomic system with four energy levels consisting of $5S_{1/2}(F=3)(|0\rangle)$, $5P_{3/2}(|1\rangle)$, $5D_{5/2}(|2\rangle)$ and $5S_{1/2}(F=2)(|3\rangle)$ as shown in Fig. 1(a). The arrangement of the experimental setup and spatial alignment of laser beams E_i(frequencyω_i and wave vector k_i) is shown in Fig. 1(c). Incident probe field E_1 with wavelength about 780.245 nm probes the transition $|0\rangle$ to $|1\rangle$. The counter-propagating fields E_3 and E_3' propagate through ^{85}Rb vapors with wavelength about 780.238 nm, connecting the transition $|3\rangle$ to $|1\rangle$. The dressing (or control) field E_2 with wavelength of 775.978 nm drives an upper transition $|1\rangle$ to $|2\rangle$. The coupling field $\boldsymbol{E}_{3s} = \hat{y}[E_3\cos(\omega_3 t - k_3 x) + E'_3\cos(\omega_3 t + k_3 x)]$, composed of E_3 and E_3', generates a standing wave. Rabi frequency of the coupling field is $G_{3s} = \mu_3 E_{3s}/\hbar$. So we have $|G_{3s}|^2 = \mu_3^2(E_3^2 + E_3'^2 + 2E_3E_3'\cos 2k_3x)/\hbar^2$. Interaction of standing wave with atomic coherent

medium results into electromagnetically induced grating. Furthermore electromagnetically induced grating will lead to a photonic band gap structure as shown in Fig. 1(b). The probe field E_1 propagates in the direction of E_3' through the ^{85}Rb vapors with approximately 0.3° angle between them. The control field E_2 propagates in the opposite direction of E_3' through ^{85}Rb with approximately 0. 3° angle between them. E_r (The reflected band gap signal from the photonic band gap structure) and E_1 is another pair of the counter-propagating beams, but with a small angle between them as shown in Fig. 1(c). Due to the small angle between E_1 and E_3', the geometry not only satisfies the phase-matching condition but also provides a convenient spatial separation of the applied laser and generated signal beams. Thus we can easily detect the generated beams which are highly directional[22]. The probe transmission signal and generated band gap signal are detected by photodiode detectors PD1 and PD2, respectively.

A block-diagram of the analogy of the behavior of modulating the photonic band gap structure with an optical transistor amplification function is shown in Fig. 1(d), where FWM BGS generated by E_1, E_3 and E_3' in the medium is analogous to the input signal a_{in} in the optical amplification experiment; enhanced FWM BGS is analogous to the output signal a_{out} and G is analogous to the gain factor of transistor. The mathematical model of this analogy is given as $a_{out} = G^* a_{in}$. E_2 is a control signal, power of which can be used to modulate the photonic band gap structure. This behavior is analogous to change the Q-point of electrical transistor.

Considering the time-dependent Schrödinger equation, using the perturbation chain $\rho_{00}^{(0)} \xrightarrow{\omega_1} \rho_{10}^{(1)} \xrightarrow{-\omega_3} \rho_{30}^{(2)} \xrightarrow{\omega_3} \rho_{10}^{(3)}$ (i.e., Liouville pathways with perturbation theory[23] and satisfying phase-matching condition) and rotating wave approximation, we can obtain a series of density matrix equations by using the way with combining the coupling method and the perturbation theory as follows

$$\frac{\partial \rho_{10}^{(1)}}{\partial t} = -d_{10}\rho_{10}^{(1)} + iG_1 e^{i\mathbf{k}_1\cdot\mathbf{x}}\rho_{00}^{(0)} + iG_2^* e^{-i\mathbf{k}_2\cdot\mathbf{x}}\rho_{20} + i\left(G_3 e^{i\mathbf{k}_3\cdot\mathbf{x}} + G_3' e^{i\mathbf{k}'_3\cdot\mathbf{x}}\right)\rho_{30} \tag{1}$$

$$\frac{\partial \rho_{30}^{(2)}}{\partial t} = -d_{30}\rho_{30}^{(2)} + iG_3'^* e^{-i\mathbf{k}'_3\cdot\mathbf{x}}\rho_{10}^{(1)} \tag{2}$$

$$\frac{\partial \rho_{10}^{(3)}}{\partial t} = -d_{10}\rho_{10}^{(3)} + iG_3 e^{i\mathbf{k}_3\cdot\mathbf{x}}\rho_{30}^{(2)} + iG_2^* e^{-i\mathbf{k}_2\cdot\mathbf{x}}\rho_{20} + i\left(G_3 e^{i\mathbf{k}_3\cdot\mathbf{x}} + G_3' e^{i\mathbf{k}'_3\cdot\mathbf{x}}\right)\rho_{30} \tag{3}$$

$$\frac{\partial \rho_{20}}{\partial t} = -d_{20}\rho_{20} + iG_2 e^{i\mathbf{k}_2\cdot\mathbf{x}}\rho_{10} \tag{4}$$

$$\frac{\partial \rho_{30}}{\partial t} = -d_{30}\rho_{30} + i\left(G_3^* e^{-i\mathbf{k}_3\cdot\mathbf{x}} + G_3'^* e^{-i\mathbf{k}'_3\cdot\mathbf{x}}\right)\rho_{10} \tag{5}$$

Where the superscript (0), (1), (2) or (3) express the perturbation order. $G_i = \mu_i E_i/\hbar$ is the Rabi frequency with transition dipole moment μ_i. $d_{10} = \Gamma_{10} + i\Delta_1$, $d_{20} = \Gamma_{20} + i\Delta_1 + i\Delta_2$, $d_{30} = \Gamma_{30} + i\Delta_1 - i\Delta_3$, frequency detuning $\Delta_i = \Omega_i - \omega_i$ (Ω_i is the resonance frequency of the transition driven by E_i). Γ_{ij} is transverse relaxation rate between $|i\rangle$ and $|j\rangle$. By solving Eqs. (1)–(5) with the steady state approximation and the condition $\rho_{00}^{(0)} = 1$ (which is reasonable since the probe field is always weak, compared with other fields), we finally obtain the first order and the third order density matrix elements $\rho_{10}^{(1)}$ and $\rho_{10}^{(3)}$. By similar method, with the perturbation chain $\rho_{00}^{(0)} \xrightarrow{\omega_1} \rho_{10}^{(1)} \xrightarrow{-\omega_3} \rho_{30}^{(2)} \xrightarrow{\omega_3} \rho_{10}^{(3)} \xrightarrow{\omega_2} \rho_{20}^{(4)} \xrightarrow{-\omega_2} \rho_{10}^{(5)}$, we can also obtain the fifth order density matrix element $\rho_{10}^{(5)}$ as follows

$$\rho_{10}^{(1)} = iG_1/[d_{10} + |G_{3s}|^2/d_{30} + |G_2|^2/d_{20}] \tag{6}$$

$$\rho_{10}^{(3)} = -iG_1G_3G_3'/[(d_{10} + |G_{3s}|^2/d_{30} + |G_2|^2/d_{20})^2 d_{30}] \tag{7}$$

$$\rho_{10}^{(5)} = iG_1G_3G_3'|G_2|^2/[(d_{10})^3 d_{30}d_{20}] \tag{8}$$

where $|G_{3s}|^2 = |G_3|^2 + |G_3'|^2 + 2G_3G_3'\cos(2k_3x)$. According to the relation $\varepsilon_0\chi E = N\mu\rho$, in which N, ε_0 are the atoms density and dielectric constant respectively, corresponding susceptibilities can be obtained as follows:

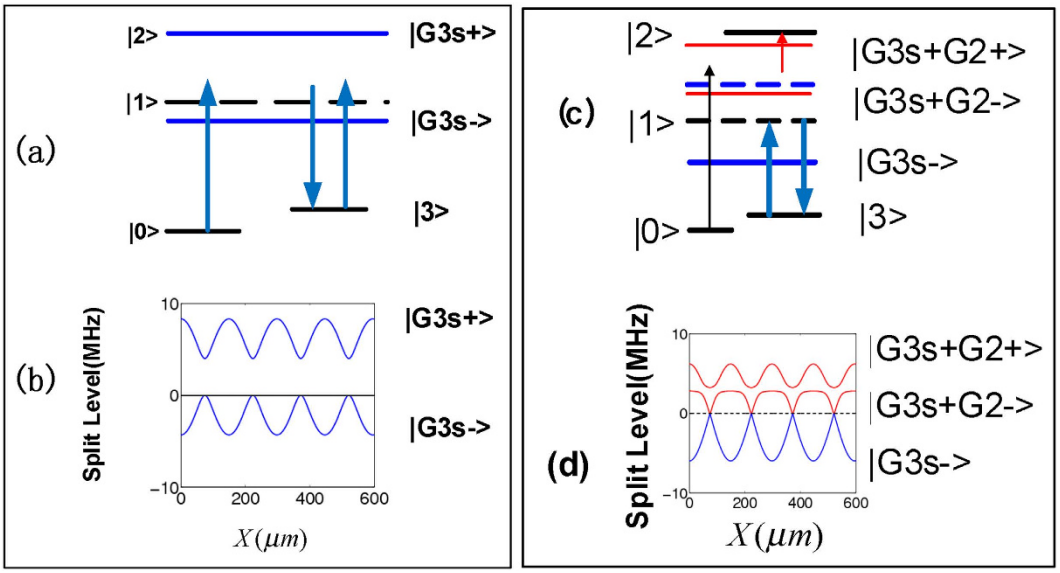

Figure 2. (**a**) The single dressed energy levels schematic diagrams and (**b**) the calculated single dressed period energy levels with changing Δ_3. (**c**) The double dressed energy levels schematic diagrams and (**d**) the calculated double dressed periodic energy levels with changing Δ_2.

$$\chi^{(1)} = iN\mu^2/[\hbar\varepsilon_0(d_{10} + |G_{3s}|^2/d_{30} + |G_2|^2/d_{20})] \tag{9}$$

$$\chi^{(3)} = -iN\mu^2/[\hbar\varepsilon_0 d_{30}(d_{10} + |G_{3s}|^2/d_{30} + |G_2|^2/d_{20})^2] \tag{10}$$

$$\chi^{(5)} = iN\mu^2/[\hbar\varepsilon_0 d_{30} d_{20}(d_{10})^3] \tag{11}$$

The condition of generating the photonic band gap structure is that the medium is of periodic refractive index. In order to get the periodic refractive index, the susceptibility should be periodic according the relation of refractive index with susceptibility, i.e., $n = \sqrt{1 + \mathrm{Re}(\chi)}$. To get periodic susceptibility we should generate the periodic energy levels structure. Hence, by introducing periodic standing wave field, we can obtain the periodic energy levels as shown in Fig. 2. In Fig. 2(a), level $|1\rangle$ will be split into two dressed states $|G_{3s}\pm\rangle$ depending on Δ_3 and $|G_{3s}|^2$. The two dressed states $|G_{3s}\pm\rangle$ have the eigenvalues $\lambda_{|G_{3s}\pm\rangle} = -\Delta_3/2 \pm \sqrt{\Delta_3^2/4 + |G_{3s}|^2}$. Since $|G_{3s}|^2$ is periodic along x, so $\lambda_{|G_{3s}\pm|}$ values are also periodic. Thus we can obtain the periodic energy levels as shown in Fig. 2(b). When the probe reaches two-photon resonance $\Delta_1 - \Delta_3 = 0$, the absorption will be suppressed, i.e. the probe transmission signal becomes strong. At the same time, the band gap signal will be suppressed correspondingly. Thus, we define $\Delta_1 - \Delta_3 = 0$ as the suppression condition. When E_2 is turn on, $|G_{3s}+\rangle$ is further split into two dressed states $|G_{3s} + G_2\pm\rangle$ due to the second level dressing effect of E_2. The two dressed states $|G_{3s} + G_2\pm\rangle$ have the eigenvalues $\lambda_{|G_{3s}+G_2\pm\rangle} = \left\{-\Delta_3 + \sqrt{\Delta_3^2 + 4|G_{3s}|^2}\right\}/2 + \left\{\Delta_2'' \pm \sqrt{\Delta_2''^2 + 4|G_2|^2}\right\}/2$ with $\Delta_2'' = \Delta_2 - \left\{-\Delta_3 + \sqrt{\Delta_3^2 + 4|G_{3s}|^2}\right\}/2$. In our system, the normalized total susceptibility is $\chi = \chi^{(1)} + \chi^{(3)}(|E_3|^2 + |E_3'|^2) + \chi^{(5)}(|E_3|^4 + |E_3'|^4 + |E_3|^2|E_3'|^2)$, which determines the refractive index of the system according to $n = \sqrt{1 + \mathrm{Re}(\chi)}$. For the system generating the band gap signal, the real part of susceptibility is periodic.

In order to estimate the reflection efficiency of band gap signal, we start with the wave equation in the following form[24],

$$\nabla^2 E - \mu_0\varepsilon_0\frac{\partial^2 E}{\partial t^2} = \mu_0\frac{\partial^2 P}{\partial t^2} \tag{12}$$

Where P is polarization of the medium given by $P = \varepsilon_0\chi(E)E$ and $E = E_0 + \Delta E$ is the total field, where $E_0 = E_3 + E_3'$ is the strong coupling fields and $\Delta E = E_r + E_1$ is the weak signal fields. Substituting P and E into Eq. (12) and using the slowly varying amplitude approximation $|d^2E_i/dx^2| \ll |k_i(dE_i/dx)|$, after

equating the coefficients of the same exponential terms on both sides of the equation, we write the propagation equations for reflected band gap signal $(E_r(x))$ and probe transmission signal $(E_1(x))$ as follows[21]

$$\partial E_1(x)/\partial x = -\alpha E_1(x) + ke^{-i\Delta k_x x}E_r(x) \tag{13}$$

$$-\partial E_r(x)/\partial x = -\alpha E_r(x) - ke^{i\Delta k_x x}E_1(x) \tag{14}$$

$\alpha = (\omega_1/c)Im\chi'^{(1)}/2$ is attenuation of the field due to the absorption of the medium and $k = i(\omega_1/c)(\chi'^{(3)} + \chi'^{(5)})/2$ is the gain due to the nonlinear susceptibilities in which four-wave and six-wave mixing are considered. $\chi'^{(1)}$, $\chi'^{(3)}$ and $\chi'^{(5)}$ are the zero order coefficients from Fourier expansion of $\chi^{(1)}$, $\chi^{(3)}$ and $\chi^{(5)}$, respectively. $\Delta k_x = \{2(\omega_1\cos\theta - \omega_3) + Re[\chi'^{(1)}]\omega_1\cos\theta\}/c$ is the phase mismatch magnitude, in which θ is the angle between probe E_1 and E_3'. Equations (13) and (14) describe the mutual generation process of $E_r(x)$ and $E_1(x)$ when they propagate inside the medium. For example, in Eq. (14), $E_1(x)$ is generating field and $E_r(x)$ is the generated field, and vice versa for Eq. (13), while $e^{i\Delta k_x x}$ represents the generating efficiency. The generating efficiency will be high when the phase matching condition is satisfied ($\Delta k_x = 0$). In order to estimate the efficiency of the reflected band gap signal and probe transmission signal, we solve Eqs. (13) and (14) as follows. We differentiate Eq. (13) with respect to x and simplify it by using Eq. (14) to get the following second order differential equation

$$\frac{\partial^2 E_1(x)}{\partial x^2} - \alpha^2 E_1(x) - k^2 E_1(x) + i\Delta k_x k e^{-i\Delta k_x x}E_r(x) = 0 \tag{15}$$

After eliminating $E_r(x)$ from Eqs. (13) and (15), we get the following equation

$$\frac{\partial^2 E_1(x)}{\partial x^2} + (-k^2 - \alpha^2 + i\Delta k_x\alpha)E_1(x) + i\Delta k_x\frac{\partial}{\partial x}E_1(x) = 0 \tag{16}$$

The general solution of Eq. (16) is $E_1(x) = B_1^{+}e^{\lambda_1^{+}x} + B_1^{-}e^{\lambda_1^{-}x}$. Next we substitute the value of $E_1(x)$ in Eq. (13) to get $E_r(x) = \frac{\lambda_1^{+}+\alpha}{k}B_1^{+}e^{\lambda_2^{+}x} + \frac{\lambda_1^{-}+\alpha}{k}B_1^{-}e^{\lambda_2^{-}x}$. Where $\lambda_1^{+} = -i\Delta k_x/2 \pm [(\alpha - i\Delta k_x/2)^2 + k^2]^{1/2}$ and $\lambda_2^{\pm} = \lambda_1^{\pm} + i\Delta k_x$. We assume that length of the ^{85}Rb sample is d_x and apply initial conditions $E_1(0) = E_0$ and $E_r(dx) = 0$ to get the values of $B_1^{+} = \frac{-(\lambda_1^{-}+\alpha)E_0e^{\lambda_2^{-}dx}}{(\lambda_1^{+}+\alpha)e^{\lambda_2^{+}dx} - (\lambda_1^{-}+\alpha)e^{\lambda_2^{-}dx}}$ and $B_1^{-} = E_0 + \frac{(\lambda_1^{-}+\alpha)E_0e^{\lambda_2^{-}dx}}{(\lambda_1^{+}+\alpha)e^{\lambda_2^{+}dx} - (\lambda_1^{-}+\alpha)e^{\lambda_2^{-}dx}}$. We define the reflection efficiency of band gap signal from the photonic band gap structure with respect to the incident probe field as

$$R = \left|\frac{E_r(0)}{E_1(0)}\right|^2 = \left|\frac{1}{k}\frac{e^{-\lambda_2^{+}d_x} - e^{-\lambda_2^{-}d_x}}{e^{-\lambda_2^{+}d_x}(\lambda_1^{+}+\alpha)^{-1} - e^{-\lambda_2^{-}d_x}(\lambda_1^{-}+\alpha)^{-1}}\right|^2 \tag{17}$$

While the probe transmission efficiency across the medium with respect to the incident probe field is defined as

$$T = \left|\frac{E_1(dx)}{E_1(0)}\right|^2 = \left|\frac{e^{(\lambda_1^{+}+\lambda_1^{-})d_x}(\lambda_1^{-} - \lambda_1^{+})}{(\lambda_1^{-}+\alpha)e^{\lambda_1^{-}d_x} - (\lambda_1^{+}+\alpha)e^{\lambda_1^{+}d_x}}\right|^2 \tag{18}$$

First, we observe the variations in the intensities of band gap signal and probe transmission signal by scanning Δ_2 at different discrete values of Δ_1 as shown in Fig. 3. Note that variations in the intensities discussed here are displayed by the efficiencies of probe transmission signal and reflected band gap signal in the following figures according to the above theory. In Fig. 3(a), each sub curve's peak is the dressed probe transmission signal induced by the second-level dressing effect of E_2, which meets the condition $\Delta_1 + \Delta_2 = 0$ according to the dressing term $|G_2|^2/d_{20}$ of Eq. (6). The smallest peak appears at $\Delta_1 = \Delta_3$ because of the strongest cascaded interaction between E_3 and E_2 as depicted by the doubly dressed term $|G_{3s}|^2/d_{30} + |G_2|^2/d_{20}$ in Eq. (6). In Fig. 3(b) the baselines show the intensity of FWM BGS, which is the reflection from photonic band gap structure. The dip in each sub curve shows that FWM BGS is suppressed while the peak within each sub curve represents that FWM BGS is enhanced. It is worth mentioning that, in the case of scanning the dressing frequency detuning Δ_2, the suppression and enhancement of FWM BGS are caused by the same dressing term $|G_2|^2/d_{20}$ of $\rho_{10}^{(3)}$ in Eq. (7), but at different positions. The suppression of FWM BGS occurs at the dark state position $\Delta_2 = -\Delta_1$ while the enhancement occurs at the bright state position $\Delta_2 = -\Delta_1 - G_2$. The six-wave mixing band gap signal whose efficiency is given by R in Eq. (17) with $k = i(\omega_1/c)\chi'^{(5)}/2$ locates at $\Delta_2 = -\Delta_1$ according to $\rho_{10}^{(5)}$ in Eq. (8), which is so weak that it is submerged in the suppression dip of FWM BGS. The expansion

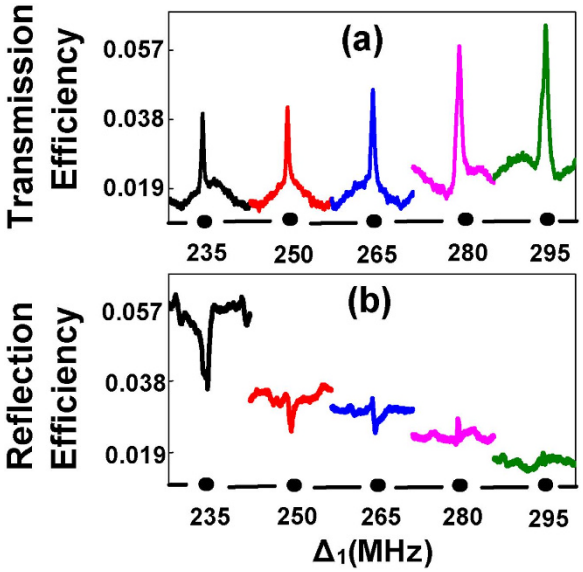

Figure 3. Measured **(a)** efficiency of probe transmission signal and **(b)** efficiency of reflected band gap signal (E_r) versus Δ_2, when we select five different discrete values of Δ_1 as black (235 MHz), red (250 MHz), blue (265 MHz), pink (280 MHz) and green (295 MHz) and $\Delta_3 = 230$ MHz. The discrete X-axis consist of solid black circles shows the different discrete designated Δ_1 for each sub-curve. Total scanning frequency range of Δ_2 in each sub-curve is about 240 MHz.

of $\rho_{10}^{(3)}$ gives us very interesting information about band gap signal, which is $\rho_{10}^{(3)} = \{-iG_1G_3G_3'[1 - 2(|G_{3s}|^2/d_{30} + |G_2|^2/d_{20})/d_{10}]\}/d_{30}d_{10}^2$. The first term is related to the intensity of baseline of FWM BGS without the dressing effect while the last term results in the suppression dip of FWM BGS at the dark state position and the enhancement peak of FWM BGS at the bright state position with the dressing effect. Enhancement of FWM BGS is used to demonstrate the analogy of an optical transistor function with the behavior of modulating the reflected band gap signal. With Δ_1 changing from small to large values, enhancement peak of FWM BGS first becomes obviously large and then at very larger detuning it becomes small again. Figure 3(b) shows that the probe detuning can be used to find the optimal conditions for the reflected band gap signal. This information can be used to give the analogy of the enhancement and suppression of the reflected band gap signal with optical amplification and switching. Maximum enhancement of band gap signal occurs at particular detuning ($\Delta_1 = 280$ MHz), while the maximum suppression occurs at $\Delta_1 = 235$ MHz, as shown in Fig. 3(b). 235 MHz and 280 MHz are the optimal values of Δ_1 which are used to demonstrate the optical switch and amplification functions.

Next, we observe the variations in the intensities of probe transmission signal and band gap signal versus dressing frequency detuning Δ_2 by blocking different beams at two optimal values of Δ_1 as shown in Fig. 4. Based on the values of Δ_1, we classify the signals in two different groups. First, Fig. 4(a1–b1),(a2–b2) shows probe transmission signal and band gap signal with no blocking and blocking E_2 when Δ_1 is set as 235 MHz. In Fig. 4(a1), when all the beams are turned on, there is a peak in the probe transmission signal because of the dressing term $|G_2|^2/d_{20}$ of $\rho_{10}^{(1)}$ in Eq. (6) which is suppressed by $|G_{3s}|^2/d_{30}$. The efficiency of the probe transmission signal is measured by T in Eq. (18). In Fig. 4(a2), the peak in the probe transmission signal disappears by blocking E_2 because of the absence of dressing term $|G_2|^2/d_{20}$ of $\rho_{10}^{(1)}$ in Eq. (6). At the moment, the height of the straight line represents the intensity of probe transmission signal caused by E_{3s} according to $\rho_{10}^{(1)}$, which is of the same intensity with the baseline of sub curve in Fig. 4(a1). To demonstrate the switching function of a transistor, the value of Δ_1 should be set as about 235 MHz. At the same time, we define the intensity of the band gap signal lower than reference level (RL) as OFF-State while the intensity higher than reference level as ON-State of the switch. Two extreme values 0 mW and 21 mW of the power of control signal (P_2) are used to turn on or off the switch. The two extreme values of P_2 are analogous to the digital values of gate voltage or base current in the case of MOSFET and BJT respectively. In Fig. 4(b2), when P_2 is set to 0 mW, the band gap signal is analogous to the input signal of a transistor. This band gap signal is FWM BGS generated by E_1, E_3 and E_3' without E_2 according to $\rho_{10}^{(3)}$ of Eq. (7) in the medium. When P_2 is set to 0 mW, the input signal directly passes to the output (the detector PD2 (Fig. 1(c))). Since the output signal intensity is higher than reference level, the switch is ON-State. When P_2 is set as 21 mW, the baseline in Fig. 4(b1) has the same intensity with the band gap signal in Fig. 4(b2). The dip shows that FWM BGS is suppressed

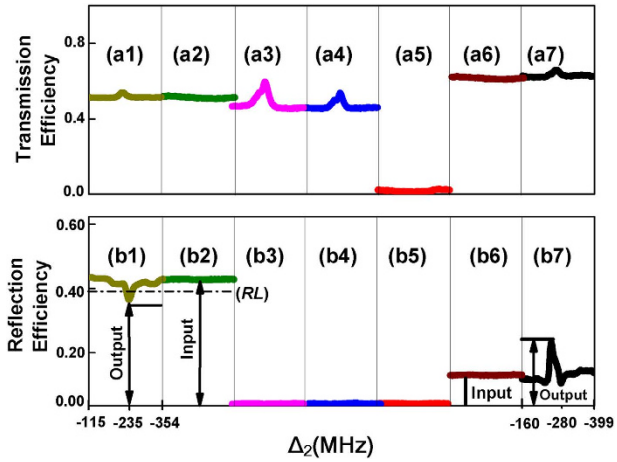

Figure 4. Measured **(a)** efficiency of probe transmission signal and **(b)** efficiency of reflected band gap signal (E_r) versus Δ_2, with $\Delta_3 = 230$ MHz when different beams are blocked. First, when $\Delta_1 = 235$ MHz, (a1) (b1) no beam blocked, (a2) (b2) E_2 blocked, RL represents reference level; Next, when $\Delta_1 = 280$ MHz, (a3) (b3) E_3 blocked, (a4) (b4) E_3' blocked, (a5) (b5) E_1 blocked, (a6) (b6) E_2 blocked and (a7) (b7) no beam blocked. Total scanning frequency range of Δ_2 in each sub-curve is about 240 MHz.

because of the dressing term $|G_2|^2/d_{20}$ of $\rho_{10}^{(3)}$ in Eq. (7). Physically, due to the modulation effect of E_2 on the photonic band gap structure at $\Delta_2 = -\Delta_1$, the reflected FWM BGS will get weak. At the moment, the output signal intensity (which is given by the lowest point of curve in Fig. 4(b1)) at the detector PD2 (Fig. 1(c)) is lower than the reference level and the switch is OFF-State. Next, from Fig. 4(a3–b3) to Fig. 4(a7–b7), we observe the variations of probe transmission signal and reflected band gap signal by blocking E_3, blocking E_3', blocking E_1, blocking E_2 and no blocking with $\Delta_1 = 280$ Mhz from left to right, respectively. The results in Fig. 4(a6,a7) are similar with the ones in Fig. 4(a1,a2). In Fig. 4(a3,a4), intensities of the peaks in the probe transmission signal increases by blocking E_3 and E_3', respectively, compared with Fig. 4(a7) (no blocking). This is because of the decreasing suppression effect of $|G_{3s}|^2$ in the cascaded dressing term $|G_{3s}|^2/d_{30} + |G_2|^2/d_{20}$ of $\rho_{10}^{(1)}$ in Eq. (6). Intensity of the probe transmission signal will become zero by blocking the incident probe beam (E_1) because of G_1 is zero in Eq. (6) as shown in Fig. 4(a5). The reflected band gap signal can be enhanced with increasing P_2 when Δ_1 is set as about 280 MHz as shown Fig. 4(b7), whose efficiency is measured by R in Eq. (17). This behavior is analogous to the amplification function of transistor. To demonstrate the analogy of the enhancement of the band gap signal with amplification function of a transistor, we need set Δ_1 as about 280 MHz. Compared with Fig. 4(b7) (no blocking), the enhancement peaks in the band gap signal disappear by blocking E_3', E_3, E_1 or E_2, respectively, as shown in Fig. 4(b3–b6). As shown in Fig. 4(b3,b4), when any one of E_3' or E_3 is blocked, the photonic band gap structure is deformed and therefore the reflected band gap signal disappears. In Fig. 4(b5), when the incident probe beam is blocked, there is still no reflection because of the absence of incident signal source E_1 according to $\rho_{10}^{(3)}$ in Eq. (7) although the photonic band gap structure is there. When E_2 is turned off, Fig. 4(b6) shows the FWM BGS generated by E_1, E_3 and E_3 according to $\rho_{10}^{(3)}$ of Eq. (7). The FWM BGS is analogous to the input signal in the optical amplification experiment. When E_2 is turned on, the FWM BGS can be obviously enhanced as shown in Fig. 4(b7). Physically, at the large detuning $\Delta_1 = 280$ Mhz, due to the modulation effect of E_2 on the photonic band gap structure at $\Delta_2 = -\Delta_1 - G_2$, the reflected FWM BGS will become strong. The highest point of peak in Fig. 4(b7) gives the amplified intensity of the band gap signal, which is the output in the optical amplification experiment. Furthermore, the baseline in Fig. 4(b7) has the same intensity with the band gap signal in Fig. 4(b6), which can also be viewed as the input signal in the optical amplification experiment. It is clear from the above discussion, to operate the system as a switch, we need set Δ_1 as about 235 MHz; while to operate it as an amplifier, we need set Δ_1 as about 280 MHz and make the power of incident probe smaller at the same time.

Next, we further demonstrate the analogy of modulating the band gap signal with the optical transistor amplification function with the power dependences of probe transmission signal and band gap signal versus Δ_2. Variations in the two types of signals are shown from right to left with increasing power of $E_2(P_2)$ as shown in Fig. 5(a1–b1). In Fig. 5(a1), the peak in each baseline shows the enhancement of the probe transmission signal induced by the dressing effect of E_2. The efficiency of the probe transmission signal is given by T in Eq. (18). The dressing term $|G_2|^2/d_{20}$ of $\rho_{10}^{(1)}$ has an enhancement effect on the probe transmission signal. Changing P_2 from small to large values, the peak becomes higher with the increasing dressing effect of $|G_2|^2/d_{20}$ in $\rho_{10}^{(1)}$ of Eq. (6). In Fig. 5(b1), the baseline of each sub curve

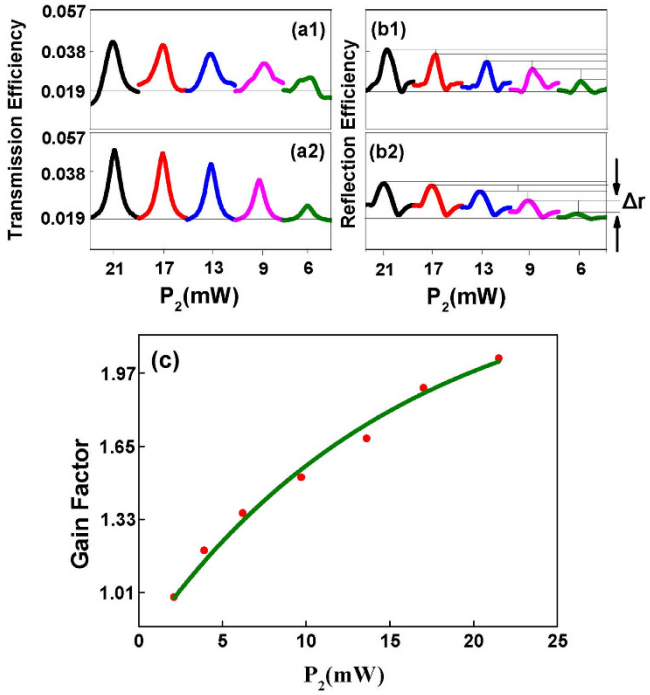

Figure 5. Measured **(a1)** efficiency of probe transmission signal and **(b1)** efficiency of enhanced four wave mixing band gap signal (E_r) versus Δ_2 from 160 MHz to 400 MHz with $\Delta_3 = 230$ MHz and $\Delta_1 = 280$ MHz, when we set the power of E_2 (P_2) as (Black) 21.5 mW, (Red) 17.0 mW, (Blue) 13.6 mW, (Pink) 9.7 mW, (Green) and 6.2 mW, respectively. (a2) and (b2) are the theoretical calculations of (a1) and (b1), respectively. (**c**) Gain factor of the amplifier versus P_2. (Solid circles are the experimental data points, while the solid line is theoretical fitting result).

shows intensity of FWM BGS generated by E_1, E_3 and E_3' which is analogous to the input signal in the optical amplification experiment according to the discussion about Fig. 4(b6,b7). Dips at $\Delta_2 = -\Delta_1$ show the suppression of reflected FWM BGS because of the dressing effect of E_2 according to the dressing term $|G_2|^2/d_{20}$ in $\rho_{10}^{(3)}$ of Eq. (7). The efficiency of FWM BGS is measured by R in Eq. (17) with $k = i(\omega_1/c)(\chi'^{(3)} + \chi'^{(5)})/2$. The dip is shallow at small value of power and becomes deeper with increasing P_2 due to the enhanced dressing effect of E_2 from right to left in Fig. 5(b1). Peaks show the enhancement of FWM BGS, the efficiency of which is also given by R in Eq. (17) with $k = i(\omega_1/c)\chi'^{(3)}/2$. The highest point on each sub curve's peak in Fig. 5(b1) is the output in the optical amplification experiment. The intensity of band gap signal increases with increasing P_2. It is important to mention here that $\rho_{10}^{(3)}$ in Eq. (7) shows that enhancement of FWM BGS at $\Delta_2 = -\Delta_1 - G_2$ is because of the dressing term $|G_2|^2/d_{20}$. Interestingly, the dressing tem $|G_2|^2/d_{20}$ is common to both $\rho_{10}^{(1)}$ and $\rho_{10}^{(3)}$. Therefore, the band gap signal with the higher intensity corresponds to the stronger probe transmission signal as shown in Fig. 5. Thus it is important to measure the probe transmission signal because of its strong relation with the band gap signal. Here we give an analogy of the amplification function of the transistor with modulating the ban gap signal. This analogy of the amplification function is demonstrated by two alternative ways which are modulating photonic band gap structure and changing the power of the incident probe field (E_1). Here we modulate the photonic band gap structure by changing the power of control signal (P_2) to get the amplified output signal, while powers of the incident probe and coupling fields are held constant, i.e. the FWM BGS generated by the probe and coupling fields is constant, which is viewed as the input here. As mentioned earlier band gap signal is the reflection of a controllable photonic band gap structure. Therefore the intensity of the reflection can be changed by controlling the photonic band gap structure or by changing power of the incident probe field (E_1). The photonic band gap structure can be controlled by changing P_2. As shown in Fig. 2(d), P_2 further modulates the periodic energy levels to change the generated photonic band gap structure. Like the electrical transistors, changing P_2 is analogous to changing biasing of electrical transistor. When the biasing of a transistor is changed, its operation point (Q-point) is shifted. As shown in Fig. 5(c), the gradient of gain factor (the ratio of the amplified band gap signal intensity (the highest point in the peak) to the original FWM BGS intensity (the baseline)) versus P_2 curve is gradually decreasing as the amplification of band gap signal tends toward saturation. Similarly the relative amount of amplification (Δr) also decreases with P_2 increasing for a fixed input signal as the bang gap signal intensity reaches the saturation region as shown in Fig. 5(b1). This behavior is similar to the variation of amplifier output by changing Q-point or biasing of a transistor.

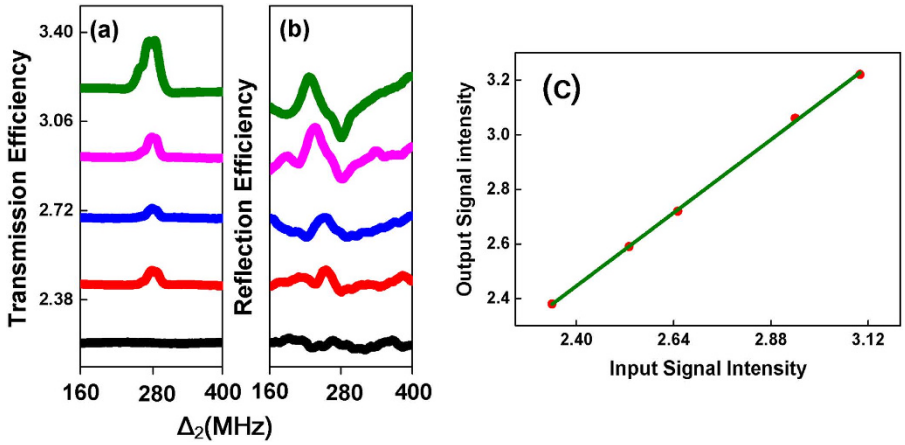

Figure 6. Measured (a) efficiency of probe transmission signal, **(b)** efficiency of enhanced four wave mixing band gap signal (E_r) versus Δ_2 with $\Delta_3 = 230$ MHz, $\Delta_1 = 280$ MHz and $P_2 = 3$ mW, when we set the power of $E_1(P_1)$ from top to bottom as (1) 2.68 mW, (2) 2.01 mW, (3) 1.10 mW, (4) 0.62 mW, and (5) 0.43 mW, respectively. (**c**) Output signal intensity (enhanced FWM BGS whose intensity is the one of the highest point on the peak of each sub curve in (**b**)) versus input signal intensity(FWM BGS whose intensity is the one of the baseline in each sub curve in (**b**)).

Figure 5(a2–b2) shows the theoretical calculations of Fig. 5(a1–b1), which are in well agreement with the experimental results.

Finally, we change the power of $E_1(P_1)$ and observe the variations in probe transmission signal and band gap signal versus Δ_2. Power dependences of the two types of signals are shown from top to bottom with decreasing power of $E_1(P_1)$ as shown in Fig. 6(a,b). The intensity of the probe transmission signal decreases with decreasing power of E_1 according to $\rho_{10}^{(1)}$ in Eq. (6). Peaks in Fig. 6(a) become smaller from top to bottom with the decreasing power of E_1 because of G_1 in Eq. (6). In Fig. 6(b), the baseline of the signal represents the intensity of the FWM BGS generated by E_1, E_3 and E_3' which is analogous to the input here according to the discussion about Fig. 4(b6,b7). Dips show the suppression of the FWM BGS because of the dressing term $|G_2|^2/d_{20}$ of $\rho_{10}^{(3)}$ in Eq. (7). The suppression is further modulated by changing P_1. The dip becomes shallow from top to bottom by changing P_1 from large to small values. Peaks in the baseline show the enhancement of the FWM BGS. The highest point on the peak gives the intensity of the amplified band gap signal, which is the output of the amplifier. Compared to the previous case where we changed the power of E_2, here the band gap signal intensity is changed by changing P_1. Since E_1 is the generating field for FWM BGS which is viewed as the input in the optical amplification experiment, the intensities of input signals increase as increasing P_1, as shown by x coordinate values of solid circles in Fig. 6(c) which are obtained by measuring the intensities of baselines of Fig. 6(b). As a result, the output intensities (the highest points on the peaks) change in proportion to the input intensities when the power of the control signal (E_2) is fixed as shown by y coordinate values of solid circles in Fig. 6(c) which are obtained by measuring the intensities of highest points of peaks in Fig. 6(b). The gradient of curve in Fig. 6(c) is constant, which is analogous to the behavior of electrical transistor operated at a fixed Q-point with a constant gain (G) due to the fixed power of the control signal (E_2) which decides the Q-point.

Discussion

In summary, the double-dressed probe transmission signal and band gap signal are compared for the first time to deeply comprehend the double-dressing effect on the photonic band gap structure. We experimentally and theoretically demonstrated that, probe transmission signal and band gap signal can be manipulated by multiple parameters like changing power and frequency detuning. We demonstrate the analogy between switching and amplification function of the transistor with modulating the reflected band gap signal. Such research could find its applications in optical diodes and transistors which are used in quantum information processing.

Methods

In our experiment, there are four laser beams generated by three external cavity diode lasers (ECDL) with line width of less than or equal to 1 MHz. The probe laser beam $\boldsymbol{E}_1$ is from an ECDL with a horizontal polarization. The two coupling laser beams $\boldsymbol{E}_3$ and $\boldsymbol{E}_3'$ with a vertical polarization are split from another ECDL. The dressing laser beam $\boldsymbol{E}_2$ with a vertical polarization is from the third ECDL. The intensity of probe beam E_1 is the only weak laser beam while other laser beams are strong. The powers of $\boldsymbol{E}_1$, $\boldsymbol{E}_3$ and $\boldsymbol{E}_3'$ are 2.1 mW, 13.2 mW and 8.4 mW, respectively. And P_2 are set as 21 mW in the experi-

ment of changing probe frequency detuning. The atomic vapor cell has the typical density of $2 \times 10^{11}\,\mathrm{cm}^{-3}$. We measure the probe transmission signal and band gap signal in the inverted Y-type four level atomic system which can be dressed by fields $\boldsymbol{E}_3(\boldsymbol{E}_3')$, $\boldsymbol{E}_2$. The four and six wave mixing band gap signals satisfy the phase-matching conditions $\mathbf{k_F} = \mathbf{k_1} + \mathbf{k_3} - \mathbf{k_3'}$ and $\mathbf{k_S} = \mathbf{k_1} + \mathbf{k_2} - \mathbf{k_2} + \mathbf{k_3} - \mathbf{k_3'}$, respectively.

References

1. Caulfield, H. J. & Dolev, S. Why future supercomputing requires optics. *Nat. Photonics* **4,** 261–263 (2010).
2. O'Brien, J. L., Furusawa, A. & Vučković, J. Photonic quantum technologies. *Nat. Photonics* **3,** 687–695 (2009).
3. Chen, W. *et al.* All-Optical Switch and Transistor Gated by One Stored Photon. *Science* **341,** 768–770 (2013).
4. Harris, S. E. Electromagnetically induced transparency. *Phys. Today*. **50,** 36–42 (1997).
5. Gea-Banacloche, J., Li, Y. Q., Jin, S. Z. & Xiao, M. Electromagnetically induced transparency in ladder-type inhomogeneously broadened media: Theory and experiment. *Phys. Rev. A* **51,** 576–584 (1995).
6. Du, Y. G. *et al.* Controlling four-wave mixing and six-wave mixing in a multi-Zeeman-sublevel atomic system with electromagnetically induced transparency. *Phys. Rev. A* **79,** 063839 (2009).
7. Hemmer, P. R. *et al.* Efficient low-intensity optical-phase conjugation based on coherent population trapping in sodium. *Opt. Lett.* **20** 982–984 (1995).
8. Lu, B., Burkett, W. H. & Xiao, M. Nondegenerate four-wave mixing in a double-Lambda system under the influence of coherent population trapping. *Opt. Lett.* **23,** 804–806 (1998).
9. Zibrov, A. S. *et al.* Transporting and time reversing light via atomic coherence. *Phys. Rev. Lett.* **88,** 103601 (2002).
10. Kolchin, P., Du, S. W., Belthangady, C., Yin, G. Y. & Harris, S. E. Generation of narrow-bandwidth paired photons: Use of a single driving laser. *Phys. Rev. Lett.* **97,** 113602 (2006).
11. Kang, H., Hernandez, G. & Zhu, Y. F. Slow-light six-wave mixing at low light intensities. *Phys. Rev. Lett.* **93,** 073601 (2004).
12. Zhang, Y. P. & Xiao, M. Enhancement of six-wave mixing by atomic coherence in a four-level inverted Y system. *Appl. Phys. Lett.* **90,** 111104 (2007).
13. Zhang, Y. P., Brown, A. W. & Xiao, M. Opening four-wave mixing and six-wave mixing channels via dual electromagnetically induced transparency windows. *Phys. Rev. Lett.* **99,** 123603 (2007).
14. Ling, H. Y., Li, Y. Q. & Xiao, M. Electromagnetically induced grating: Homogeneously broadened medium. *Phys. Rev. A* **57,** 1338–1344 (1998).
15. Bajcsy, M., Zibrov, A. S. & Lukin, M. D. Stationary pulses of light in an atomic medium. *Nature* **426,** 638–641 (2003).
16. Zhang, Y. P. *et al.* Four-Wave Mixing Dipole Soliton in Laser-Induced Atomic Gratings. *Phys. Rev. Lett.* **106,** 093904 (2011).
17. Wu, J. H., Artoni, M. & La Rocca, G. C. Non-hermitian degeneracies and unidirectional reflectionless atomic lattices. *Phys. Rev. Lett.* **113,** 123004 (2014).
18. Artoni, M. & La Rocca, G. C. Optically tunable photonic stop bands in homogeneous absorbing media. *Phys. Rev. Lett.* **96,** 073905 (2006).
19. Schilke, A., Zimmermann, C., Courteille, P. W. & Guerin, W. Photonic band gaps in one-dimensionally ordered cold atomic vapors. *Phys. Rev. Lett.* **106,** 223903 (2011).
20. Gao, M. Q. *et al.* Modulated photonic band gaps generated by high-order wave mixing. *J. Opt. Soc. Am. B* **32,** 179–187 (2015).
21. Wang, D. W. *et al.* Optical Diode Made From a Moving Photonic Crystal. *Phys. Rev. Lett.* **110,** 093901 (2013).
22. Yuan L. *et al.* Coherent Raman Umklappscattering. *Laser Phys. Lett.* **8,** 736–741 (2011).
23. Zhang, Y. & Xiao, M. Multi-Wave Mixing Processes: From Ultrafast Polarization Beats to Electromagnetically Induced Transparency (*HEP & Springer*, 2009).
24. Abrams, R. L. & Lind, R. C. Degenerate four-wave mixing in absorbing media. *Opt. Lett.* **2,** 94–96 (1978).

Acknowledgments

This work was supported by the 973 Program (2012CB921804), NSFC (61108017, 11474228), KSTIT of Shaanxi Province (2014KCT-10), NSFC of Shaanxi Province (2014JZ020), FRFCU (2012jdhz05, xjj2012080), CPSF (2015T81030, 2014M560779) and Postdoctoral research project of Shaanxi Province.

Author Contributions

Z.G.W., Z.U. and Y.P.Z. provided the idea and main contributions to the theoretical and experimental analysis of this work. M.Q.G., D.Z., Y.Q.Z. and H.G. contributed to the presentation and execution of the work. All authors discussed the results and contributed to writing the manuscript.

Additional Information

Competing financial interests: The authors declare no competing financial interests.

How to cite this article: Wang, Z. *et al.* Analogy of transistor function with modulating photonic band gap in electromagnetically induced grating. *Sci. Rep.* **5**, 13880; doi: 10.1038/srep13880 (2015).